High fidelity, high yield production of microfluidic devices by hot embossing lithography : Rheology and stiction

Cameron, Neil S.; Roberge, Helene; Veres, Teodor; Jakeway, Stephen C.; Crabtree, H. John

Publisher's version / Version de l'éditeur:
https://doi.org/10.1039/b600584e
Lab on a chip, 6, 7, pp. 936-941, 2006-04-21

High fidelity, high yield production of microfluidic devices by hot embossing lithography: rheology and stiction

Neil S. Cameron,*[a] Helene Roberge,[a] Teodor Veres,[a] Stephen C. Jakeway[b] and H. John Crabtree[b]

Received 17th January 2006, Accepted 21st April 2006
First published as an Advance Article on the web 16th May 2006
DOI: 10.1039/b600584e

We discuss thermoforming of thermoplastic polymers for the hot-embossing lithographic (HEL) fabrication of microfluidic chips near equilibrium conditions that minimize elastic recoil for optimal motif replication. While HEL is often simplistically described as the transfer of micro- and nano-motifs into heat-softened thermoplastic materials, we describe our rational approach to selecting appropriate processing parameters.

Introduction

The increasing demand for polymer-based devices as well as for low-cost micro- and nano-fabrication technologies requires the development of reproducible protocols for manufacturing using inexpensive materials. Replication of micro- and nanostructures with polymers is an active area of research, often employing injection moulding and hot embossing.[1] A good example of the utility of hot embossing is in the fabrication of chips for micro total analysis systems (μTAS), where flow channels, reservoirs and mixing chambers can be designed and fabricated directly in a single-layer polymer chip. The micro electromechanical systems (MEMS) research community has recently adopted these technologies for the replication of precision plastic/metallic microstructures, and to develop low cost mass-production-compatible microfabrication techniques for the commercialization of MEMS devices.[2] Many thermoplastic polymers have been investigated as candidate materials for such applications, including poly(methyl methacrylate) (PMMA), poly(cyclic olefin) (PCO or COC), polycarbonate (PC), poly(tetrafluoroethylene) (PTFE), polystyrene (PS) and others (Table 1).[3–5]

Polymer hot embossing is an attractive alternative for the replication of micro and sub-micro features in thermoplastic materials with dimensions from a few nanometres to several centimetres.[6,7] Motifs include vias, cruciform electrophoretic channels, mixing chambers, serpentine races and retention posts. Standard micro- and nano-fabrication techniques are employed to generate stamps. The resulting devices are characterized by SEM as well as contact and/or optical profilometry.

HEL and the glass transition

It is convenient, though deceptively simple, to describe the embossing process as the transfer of motifs into a polymer film heated above its glass transition temperature (T_g). Nevertheless, once transfer has been accomplished, the stamp and the film are separated and post-embossing processing releases functional devices. Careful stamp design[6] and judicious application of release agents[8] are necessary for successful motif replication, but the embossing process itself is rich in rheological and interfacial phenomena. Choosing appropriate processing parameters is therefore critical for high fidelity and high yield production of bioMEMS by HEL.

Displacing polymers in thin films is often treated purely in terms of T_g, viscocity and the characteristic relaxation time, τ.[9] In fact, these parameters are somewhat complicated and among the first operational parameters to be determined is an optimal embossing temperature. Visco-elastic systems do not behave as classical Newtonian fluids at or near the glass transition. A purely elastic response obeys Hooke's law where the reversible displacement is a function of force and the spring constant. A purely viscous response, on the other hand, is described by Newton's law where the stress equals the shear rate corrected by the viscocity of the material. Canonical bulk

Table 1 Selected polymer properties and embossed structures (50 μm channel width)

Polymer/Grade	T_g[a]/°C	T_{emb}/°C	Melt-flow[b]/ g per 10 min	Light trans.[c] (%)
PMMA: PMMA 100	98.8	130	105	92
PC: 1080 (Dow)	141.8	170	80	91
PCO: Zeonor 750R	72.2	110	27	92
PCO: Zeonor 1020R	104.9	150	20	92
PCO: Zeonor 1060R	104.5	140	60	92
PCO: Zeonor 1600R	165.6	200	7	92

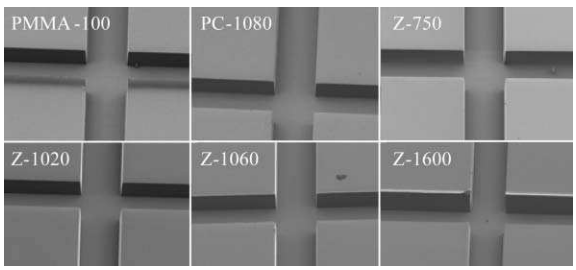

[a] TA-Q1000 DSC at 20 °C min^{-1}. [b] Various standards. [c] Commercial values.

[a]*Industrial Materials Institute: National Research Council Canada, 75 Blvd. De Mortagne, Boucherville, Québec, J4B 6Y4, Canada. E-mail: neil.cameron@cnrc.gc.ca; Fax: +1 (450) 641-5105; Tel: +1 (450) 641-5168*
[b]*Micralyne Inc., 1911-94 Street, Edmonton, Alberta, T6N 1E6, Canada. E-mail: sjakeway@micralyne.com; Fax: +1 (780) 431-4422; Tel: +1 (780) 431-4419*

and thin-film thermoplastic polymers are neither perfectly elastic nor perfectly viscous due to their chain-like structure. For any given polymer, each response is attenuated by the other to varying degrees, depending largely on the temperature of the system.[10] Above the glass transition temperature, significant segmental motion of the polymer chains renders possible a viscous response to an applied stress. Thermoplastic polymers undergo three regime transitions as they are heated from the *glassy* state below the T_g, through the *leathery* phase during the T_g transition, to a visco-elastic *rubbery* plateau until sufficient energy is supplied and the elastic response is completely dominated by *viscous flow*. The temperature range of the rubbery plateau is polymer and chain-length dependent. Clearly, the optimal embossing temperature is above T_g at the cusp of the viscous regime, where the relaxation time of the polymer, τ, is exceedingly fast and where residual stresses caused by the thermoforming of the polymer will be minimized in the absence of a rapid 'quenched' cooling step.[11,12] Arbitrary embossing values such as $T_{emb} = (T_g + n)$ °C (where n is a universal integer) are most unlikely to provide optimal embossing conditions.

Careful optimization of the process parameters, especially the embossing temperature (T_{emb}), is required to avoid damaging the embossing stack, as well as to avoid trapping residual stress and subsequent rebound,[13] and also to avoid unduly long cycle times caused by excessive heating and cooling. Choosing by how much the embossing temperature should exceed the T_g is a compromise between the reduction in the polymer moduli that facilitate faithful motif replication and the potential damage to stamp and substrate caused by longer cycle times and greater thermal distortion.

Hot embossing process

The embossing process is shown schematically in Fig. 1. Initially, a textured stamp is pressed into a heat softened polymer, and the force required for the micro-transport of displaced polymer scales with the contact area of the stamp features with the polymer (Fig. 1-i). As the stamp progresses into the substrate, the material displacement may, in principle, be purely viscous or elastic. In practice, however, the response is usually both (Fig. 1-ii, middle). Various idealized representations of the filling mechanism have been presented,[9,14] however most agree that once the stamp cavities are filled, then the embossing force scales with the entire contact area with a correction factor for the long-range transport of polymer to the edge of the stamp (Fig. 1-iii). Elucidating the details of the embossing process is not trivial, especially in the nano-regime, and instrumented approaches such as one-dimensional surface probe microscopy[8] and indentation are useful techniques to explore the development of micro- and nano-motifs.[15]

The most complicated regime occurs when the residual film thickness between the stamp motifs and the support underlayer approaches the polymer coil dimension. Polymers physisorb to silicon and silicon oxide surfaces as a function of the interfacial interaction. In the case of PMMA on a SiO_2 surface, dipole–dipole and H-bonding interactions effectively tether the polymer to the surface. The polymer conformation in this state may be described as the sum of trains (chains 'lying' on the surface), loops (segments between trains) and tails (loose ends).[16] We and others have observed an important increase in T_g at this interface for this system. Where the interaction is not favourable, for example when a non-polar polymer is coated on native SiO_2 on a silicon wafer, the polymer conformation tends to favour loops, with the concomitant increase in free-volume and subsequent *decrease* in apparent T_g.[17–24] This phenomenon has been explored for thermomechanical data storage in polymer thin-films.[25]

The final, and often most challenging, phase of the embossing cycle is the separation of stamp and substrate, since the two have been pressed together at elevated temperatures and forces in evacuated chambers to assure conformality. Anti-stiction agents such as the hydroperfluorosilanes are

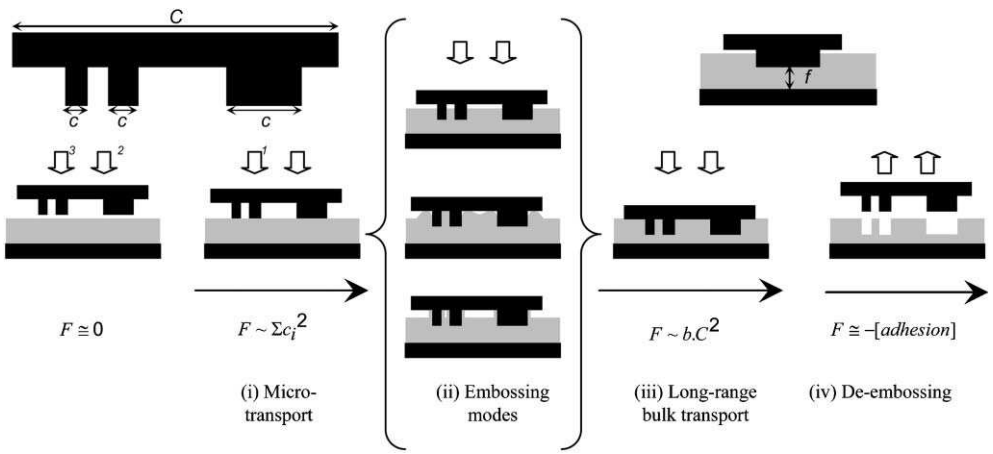

Fig. 1 The total force required to emboss a thermoplastic polymer (F) depends on the polymer's viscosity, volume to be displaced, film thickness and temperature. When positive motifs are brought into contact with the polymer above T_g, F scales with the contact area (i). The transitional mechanism (ii) sits in the spectrum of visco-elastic behaviour (observed mechanism, ii-middle; idealized schematics, ii-upper and ii-lower) and the annealing period for successful HEL must account for the polymer relaxation time, τ. When the stamp is fully embossed (*i.e.* no further short-range transport is possible), the force required to effect long-range displacement of the polymer scales with the surface area of the entire stamp (C^2) with a correction for the long-range bulk transport of polymer chains (iii). For supported thin films, F becomes very high as the residual thickness, f, approaches values below the radius of gyration of the polymer chains (iii). De-embossing occurs when the force of adhesion is overcome (iv).

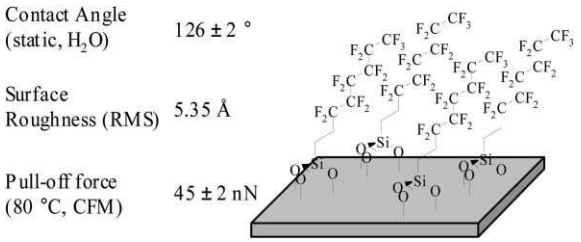

Fig. 2 Release layer characterization and idealized representation for 1,1,2,2-tetrahydroperfluorooctylsilane. Contact angles were measured with the submerged-point technique, surface roughness (RMS) was determined for the silane SAM on a silicon substrate, and pull-off force was determined for a silane-decorated SPM tip at a Zeonor 750R (PCO) interface.

routinely applied to the stamp (Fig. 2), as described in detail elsewhere.[8,26]

The smallest motifs we routinely replicate by HEL are less than 100 nm in critical dimension,[7,27] and substrate film thicknesses vary from a few tens of nm to more than a few mm. In this preliminary study, we present our interpretation and optimization of the replication of micro-motifs for lab-on-plastic-chip applications.

Experimental

Stamp fabrication

Two different families of stamps were prepared, one based on 100 mm diameter silicon wafers, and the other on 150 mm diameter electroformed nickel shims. Since the resulting embossed devices were indistinguishable, we refer to them interchangeably here. Silicon wafer stamps (100 mm) were patterned with standard photolithographic techniques and 20 μm or 50 μm deep channels were prepared with cryo deep reactive ion etching (cryo-DRIE). The wafers were backed with 5 mm thick Pyrex wafers attached with Loctite 3011 adhesive. Electroformed stamps (150 mm) were prepared by fabricating a 'negative' master in silicon from the design shown in Fig. 3. A thin-film of nickel-chrome was evaporated onto the surface followed by electrodeposition to a final thickness of 2 mm (Galvanoform, Germany). Care was taken to avoid undercuts in the final stamp that would make de-embossing impossible. The silicon master was removed, releasing a 'positive' metallic stamp. The silicon stamps were treated with 1,1,2,2-tetrahydroperfluorotrichlorosilane in the vapour-phase to facilitate de-embossing.[8]

Hot embossing

All hot embossing was carried out on an EVG 520 HE tool resembling a wafer bonder, and designed to handle both substrates and stamps up to 200 mm in diameter. The maximum operating temperature and embossing force of the instrument were 300 °C and 40 kN respectively. Heating and cooling modules were active on both the upper and lower embossing plates.

Parameter matrix

Each polymer tested for embossing was subjected to a parameter matrix in which the embossing *force* (F_{emb}), embossing *time* at the embossing plateau (t_{emb}) and *de-embosssing temperature* (T_d) were held constant at reasonable values and the *embossing temperature* (T_{emb}) was optimized empirically. With T_{emb} fixed, the optimal F_{emb} was determined. Finally, the minimum t_{emb} was determined for faithful replication of motifs. SEM micrographs were obtained for the resulting devices, and motifs were evaluated with respect to edge filling, propagating rim and stiction artifacts as illustrated in Fig. 4. Although various quantitative techniques may be applied to this process, a simple classification system (poor/fair/good) was sufficient to guide us to optimal parameters.

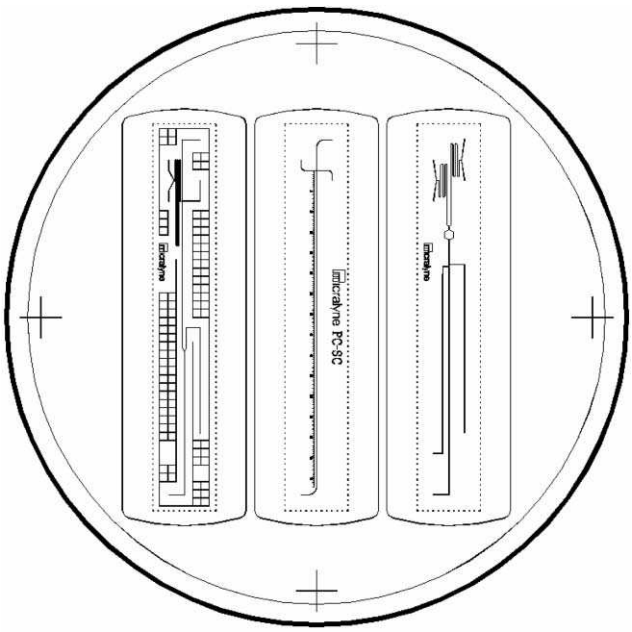

Fig. 3 Stamp design containing three different microfluidic devices.

Thermal analysis

Bulk glass transition temperatures were determined with a Thermal Analysis Q1000 modulated differential scanning calorimeter (MDSC) in classical DSC mode (Table 1). Thermal history was normalized for all samples by raising the temperature well above T_g and then cooling to room

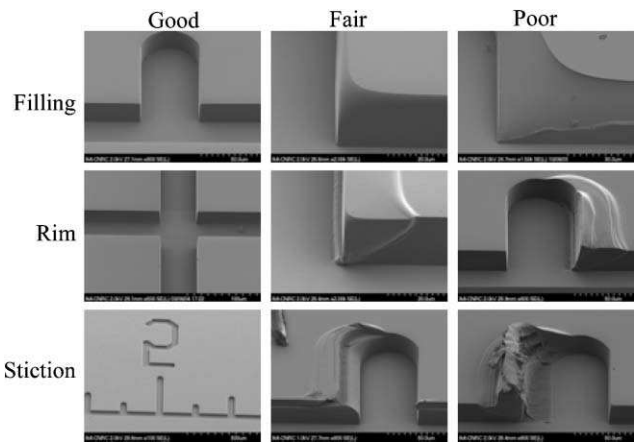

Fig. 4 Embossing evaluation matrix (channel width 50 μm).

temperature at a rate of 20 °C min^{-1}. The samples were heated at a rate of 20 °C min^{-1} and T_g was calculated from the resulting data.

Storage (E') and loss (E'') moduli as well as the loss tangent (tan δ) for Zeonor 750R and Zeonor 1060R (commercial PCO) were determined at 1 Hz, strain = 0.2%, heating rate = 2 °C min^{-1} with a Rheometric Scientific Dynamic Mechanical Thermal Analyzer (DMTA) V.

Results and discussion

Embossing parameters

The empirical determination of optimal embossing parameters can be an extraordinarily expensive proposition unless reasonable initial boundary conditions are applied. As indicated in the sample Zeonor 750R (T_g = 72.2 °C) parameter matrix (Fig. 5), at T_{emb} = T_g + 8 °C, we observed partial motif transfer and only at 110 °C, 38 °C above T_g, did we achieve complete edge filling without a propagating rim and without stiction artefacts.

Similarly, having identified an optimal T_{emb} we confirmed an appropriate F_{emb} for a 100 mm stamp holding one device. As one might expect due to the superposibility principle, lower forces (2 kN, 4 kN) were insufficient to achieve complete edge filling. At 6 and 8 kN, we observed faithful motif replication. Moderately higher embossing forces improved the replication uniformity without incurring rebound or elastic response defects.

Since our embossing cycle routinely involves a heating ramp of 10 °C per minute and a much slower cooling ramp of 1–2 °C per minute, the actual residence time at the embossing plateau was unsurprisingly non-critical. Nevertheless, one minute plateaux were determined to be insufficient for Zeonor 750R as indicated by slightly rounded corners.

Prioritizing T_{emb}, F_{emb}, and t_{emb} is often determined by the device to be fabricated and the required yield. Cycle times can be reduced by increasing the embossing force, but in the absence of an appropriate annealling step, residual stresses can be trapped in the material. Higher embossing temperatures reduce the viscosity of the polymer melt and allow for lower forces and shorter embossing plateaux, however the consequences include heat damage, thermal expansion and longer cycles due to increased temperature ramp time. We favoured gentle embossing parameters, maintaining the substrate as close to thermodynamic equilibrium as possible at all times.

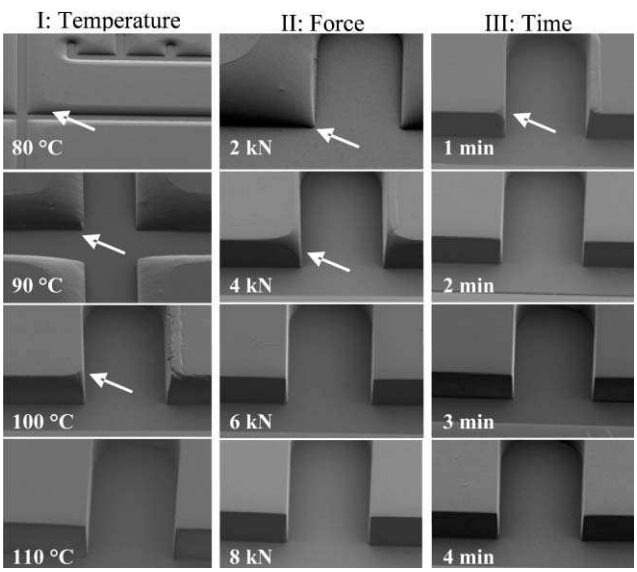

Fig. 5 Effect of embossing temperature (I), embossing force (II) and embossing time (III) on Zeonor 750 R, a poly(cyclic olefin). For the temperature series (I), the static embossing parameters were force (F_{emb}) = 7 kN, embossing time (t_{emb}) = 5 min and the de-embossing temperature (T_d) = 60 °C. For the embossing force series, the static parameters were: embossing temperature (T_{emb}) = 110 °C, t_{emb} = 5 min and T_d = 60 °C. For the embossing time series, the static parameters were: T_{emb} = 110 °C, F_{emb} = 8 kN, and T_d = 60 °C (channel width 50 μm).

Correlation with DMTA

Thermoplastic lab-on-chip devices require high-modulus materials at ambient conditions and low-modulus materials under embossing conditions. The storage (E') and loss (E'') moduli, as shown in Fig. 6, provide data for the rational choice

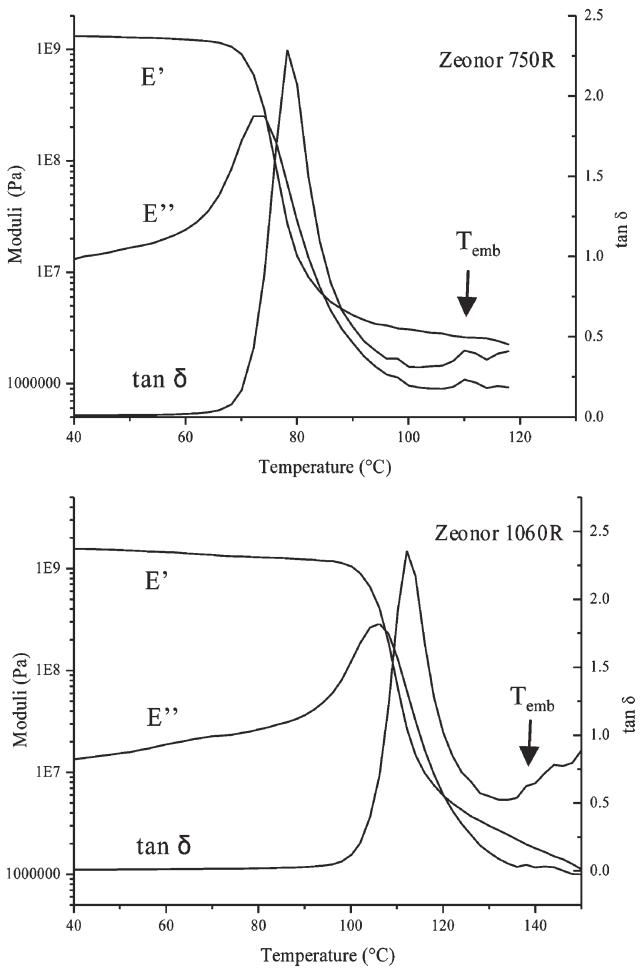

Fig. 6 Storage (E') and loss (E'') moduli as well as the loss tangent (tan δ) for the commercial poly(cyclic olefins) Zeonor 750 R and Zeonor 1060 R. Data measured at 1 Hz, strain = 0.2%, heating rate = 2 °C min^{-1} on a Rheometric Scientific DMTA V.

Table 2 Contact profilometry of silicon stamp and resulting device (RMS roughness = 30 Å)

Channel position	Beginning	Middle	End
Silicon stamp (feature height/μm)	22.030 ± 0.002	21.040 ± 0.0004	22.560 ± 0.001
Polymer chip (feature depth/μm)	22.090 ± 0.014	21.090 ± 0.038	22.680 ± 0.007

of T_{emb}. E' is a measure of the stored energy and E'' refers to the energy dissipated by the polymer when a dynamic strain is applied. The loss tangent (tan δ) is the ratio $E''(\omega)/E'(\omega)$ and describes the damping of the system. Maxima in this value indicate a change in molecular, polymer or segmental motion such as the glass or melting transitions. The single peak indicates a single relaxation process in these temperature ranges. We typically emboss Zeonor 750R and Zeonor 1060R at 110 °C and 140 °C respectively. As indicated in Fig. 6, these temperatures correspond to the cusp of the viscous regime where the viscous component of the polymer behaviour is dominant and the forces measured correspond to masses below the detection limit of the instrument. Therefore DMTA provides a means to target optimal embossing temperatures in polymer films that behave as bulk materials.

Fidelity of replication

Replication fidelity can be extraordinarily good with optimal embossing parameters. As indicated by the contact profilometry data in Table 2, stamp features on the order of 20 μm high are transferred almost perfectly into the thermoplastic polymer. The resulting slightly deeper trench dimensions are due to the compression and rebound of the polymer during the embossing cycle. Optical profilometry, as shown in Fig. 7, is also a useful method for the rapid and non-destructive characterization of microfluidic motifs including cruciform structures, splitters and serpentine races.

Conclusions

Hot embossing of microfluidic devices provides enormous parameter space for optimization. The micro- and nano-displacement of thermoplastic polymers above their T_g offers a rich mechanism for the study of micro- and nano-rheology and underscores the need for further examination of related interfacial phenomena. While brute-force optimization matrices and rule-of-thumb equations may yield acceptable embossing parameters, DMTA data provide clear indications for optimal T_{emb}. Correlation among the embossing parameters remains to be fully determined, though with our EVG520HE, the overall cycle-time ($\sim$30 minutes) is somewhat limiting in this regard. However, with a rationally selected embossing temperature and minimal variation in t_{emb}, the optimal embossing force is the only remaining significant process parameter to be determined with our tool. Our primary criterion was the high fidelity replication of microfluidic motifs while minimizing the embossing temperature and force. High throughput is assured by the massive parallelization that is possible with this lithographic method. Process optimization and interfacial science notwithstanding, HEL is a powerful technique for the high fidelity replication of micro- and nano-motifs from micro- and nano-fabricated stamps.

Fig. 7 Optical profilometry of embossed devices (Zeonor 1060R): cruciform structure (left), splitter (middle) and serpentine race (right), structure depth = 20 μm , channel width 50 μm.

Acknowledgements

The authors are grateful for financial support for the IMI-Micralyne partnership from IRAP-PARI and for technical support from Arnaud Ott, Yves Simard and Pierre Sammut. SCJ thanks the NRC for an IRF award. NSC is grateful for fruitful discussions with Dr G. Cross (Trinity College Dublin).

References

1 B. D. Gates, Q. Xu, M. Stewart, D. Ryan, C. G. Willson and G. M. Whitesides, *Chem. Rev.*, 2005, **105**, 1171–1196.
2 www.micralyne.com, www.nilfab.com, www.nilcom.org.
3 M. L. Hupert, M. A. Witek, Y. Wang, M. W. Mitchell, Y. Liu, Y. Bejat, D. E. Nikitopoulos, J. Goettert, M. C. Murphy and S. A. Soper, *Proc. SPIE–Int. Soc. Opt. Eng.*, 2003, **4982**, 52–64.
4 P. Bley, 'Micromachined Devices and Components V', *Proc. SPIE – Int. Soc. Opt. Eng.*, Santa Clara, CA, USA, 1999.
5 M. W. Mitchell, X. Liu, Y. Bejat, D. E. Nikitopoulos, S. A. Soper and M. C. Murphy, 'Microfluidics, BioMEMS, and Medical Microsystems', *Proc. SPIE – Int. Soc. Opt. Eng.*, San Jose, CA, USA, 2003.
6 M. Esch, S. Kapur, G. Irizarry and V. Genova, *Lab Chip*, 2003, **3**, 121–127.
7 S. Y. Chou, P. R. Krauss and P. J. Renstrom, *Appl. Phys. Lett.*, 1995, **67**, 3114.
8 N. S. Cameron, A. Ott, H. Roberge and T. Veres, *Soft Matter*, 2006, DOI: 10.1039/b600936k.
9 H.-C. Scheer and H. Schultz, *Microelectron. Eng.*, 2001, **56**, 311–332.
10 J. M. G. Cowie, *Polymers: Chemistry and Physics of Modern Materials*, Chapman & Hall, New York, 1994.
11 A. Eisenberg, in *Physical Properties of Polymers*, 1984, pp. 54–95.
12 D. J. Plazek and K. L. Ngai, in *Physical Properties of Polymers Handbook*, ed. J. E. Mark, AIP Press, New York, 1996, vol. 1, pp. 139–159.
13 G. L. W. Cross, B. S. O'Connell and J. B. Pethica, *Appl. Phys. Lett.*, 2005, **86**, 081902.
14 G. L. W. Cross, R. M. Langford, B. S. O'Connell and J. B. Pethica, *Mater. Res. Soc. Symp. Proc.*, 2005, **841**, R1.6.1–12.
15 G. L. W. Cross, B. S. O'Connell, J. B. Pethica, H. Schultz and H. C. Scheer, *Microelectron. Eng.*, 2005, **78–79**, 618–624.
16 L. A. Utracki, *Clay-containing polymeric nanocomposites*, Rapra Technology Limited, Shrewsbury, 2004.
17 N. S. Cameron, H. Roberge, T. Veres, S. C. Jakeway and H. J. Crabtree, *Polymer Processing Society Americas Regional Meeting*, Quebec, Canada, 2005.
18 J. A. Forrest and K. Dalnoki-Veress, *Adv. Colloid Interface Sci.*, 2001, **94**, 167–196.
19 O. Prucker, S. Christian, H. Bock, J. Rühe, C. W. Frank and W. Knoll, *Macromol. Chem. Phys.*, 1998, **199**, 1435–1444.

20 R. A. L. Jones, *Curr. Opin. Colloid Interface Sci.*, 1999, **4**, 153–158.
21 R. S. Tate, D. S. Fryer, S. Pasqualini, M. F. Montague, J. J. de Pablo and P. F. Nealey, *J. Chem. Phys.*, 2001, **115**, 9982–9990.
22 D. S. Fryer, R. D. Peters, E. J. Kim, J. E. Tomaszewski, J. J. de Pablo, P. F. Nealey, C. C. White and W.-l. Wu, *Macromolecules*, 2001, **34**, 5627–5634.
23 J. H. van Zanten, W. E. Wallace and W.-l. Wu, *Phys. Rev. E*, 1996, **53**, R2053–R2055.
24 S. Sills, R. M. Overney, W. Chau, V. Y. Lee, R. Miller and J. Fromer, *J. Chem. Phys.*, 2004, **120**, 5334–5338.
25 G. L. W. Cross, M. Despont, U. T. Dürig, K. E. Goodson, W. P. King, H. Rothuizen, G. K. Binnig and P. Vettiger, personal communication.
26 H. Schift, S. Saxer, S.-G. Park, C. Padeste, U. Pieles and J. Gobrecht, *Nanotechnology*, 2005, **16**, S171–S175.
27 W. Wu, B. Cui, X.-y. Sun, W. Zhang, L. Zhuang, L. Kong and S. Y. Chou, *J. Vac. Sci. Technol., B*, 1998, **16**, 3825–3829.